Marine Geology 387 (2017) 45–57

Contents lists available at ScienceDirect

Marine Geology

journal homepage: www.elsevier.com/locate/margo

Seasonal hypoxia was a natural feature of the coastal zone in the Little Belt, Denmark, during the past 8 ka

Niels A.G.M. van Helmond[a,*], Nadine B. Quintana Krupinski[b], Bryan C. Lougheed[c], Stephen P. Obrochta[d], Thomas Andrén[e], Caroline P. Slomp[a]

[a] Geochemistry, Department of Earth Sciences, Faculty of Geosciences, Utrecht University, Princetonplein 9, 3584 CC Utrecht, Netherlands
[b] Department of Geology, Lund University, SE-223 62 Lund, Sweden
[c] Department of Earth Sciences, Uppsala University, Villavägen 16, 75236 Uppsala, Sweden
[d] Graduate School of International Resource Science, Akita University, 1-1 Tegata Gakuin-cho, Akita 010-8502, Japan
[e] School of Natural Sciences, Technology and Environmental Studies, Södertörn University, SE-141 89 Huddinge, Sweden

ABSTRACT

The extent of the hypoxic area in the Baltic Sea has rapidly expanded over the past century. Two previous phases of widespread hypoxia, coinciding with the Holocene Thermal Maximum (HTM; 8–4 ka before present; BP) and the Medieval Climate Anomaly (MCA; 2–0.8 ka BP), have been identified. Relatively little is known about bottom water redox conditions in the coastal zone of the Baltic Sea during the Holocene, however. Here we studied the geochemical composition of a sediment sequence from a currently seasonally hypoxic site in the Danish coastal zone, the Little Belt, retrieved during Integrated Ocean Drilling Program Expedition 347 (Site M0059). The base of the studied sediment sequence consists of clays low in organic carbon (C_{org}), molybdenum (Mo) and iron sulfides (Fe-sulfides), and rich in iron oxides (Fe-oxides), indicative of a well-oxygenated, oligotrophic (glacial) meltwater lake. An erosional unconformity separates the glacial lake sediments from sediments that are rich in C_{org}. The absence of Mo, in combination with high C_{org}/S values, indicates that these sediments were deposited in a highly productive, well-oxygenated freshwater lake. The transition to modern brackish/marine conditions was very rapid, and subsequent continuous sequestration of Mo in the sediment and high ratios of reactive iron (Fe_{HR}) over total Fe (Fe_{TOT}) suggest (seasonal) hypoxia occurred over the last ~8 ka. Maxima in sediment C_{org}, Mo and Fe_{HR}/Fe_{TOT} ratios during the HTM and MCA suggest that the hypoxia intensified. Our results demonstrate that the Little Belt is naturally susceptible to the development of seasonal hypoxia. While periods of climatic warming led to increased deoxygenation of bottom waters, high nutrient availability in combination with density stratification were likely the main drivers of hypoxia in this part of the coastal zone of the Baltic Sea during the Holocene.

1. Introduction

Dissolved oxygen concentrations have been decreasing in many parts of the world's oceans over the past decades (e.g. Whitney et al., 2007; Stramma et al., 2008; Karstensen et al., 2015). Particularly coastal bottom waters are increasingly suffering from hypoxia, i.e. dissolved oxygen concentrations < 2 mg/L (Diaz and Rosenberg, 2008). The expansion of coastal hypoxia has led to a decreasing diversity of benthic communities, fish habitat loss and the development of benthic dead zones (e.g. Rabalais et al., 2002; Diaz and Rosenberg, 2008; Vaquer-Sunyer and Duarte, 2008). Increased anthropogenic nutrient input is the primary cause of deoxygenation in coastal waters (e.g. Diaz and Rosenberg, 2008), which can be further enhanced by global warming through its impact on gas solubility, water column ventilation and enhanced marine primary productivity (e.g. Keeling et al., 2010; Carstensen et al., 2014a; Hallegraeff, 2010).

The Baltic Sea is a prime example of a basin where bottom water hypoxia has expanded due to human activities (Gustafsson et al., 2012) and has been amplified due to climatic warming (Kabel et al., 2012; Carstensen et al., 2014a). Over the past century, the hypoxic area in the Baltic Sea has increased tenfold (Carstensen et al., 2014a), consequently leading to major changes in the abundance and spatial distribution of benthic fauna (Karlson et al., 2002; Conley et al., 2009). The Baltic Sea is particularly sensitive to hypoxia because of its estuarine circulation

* Corresponding author.
E-mail addresses: n.vanhelmond@uu.nl (N.A.G.M. van Helmond), nadine.krupinski@geol.lu.se (N.B. Quintana Krupinski), bryan.lougheed@geo.uu.se (B.C. Lougheed), obrochta@gipc.akita-u.ac.jp (S.P. Obrochta), thomas.andren@sh.se (T. Andrén), c.p.slomp@uu.nl (C.P. Slomp).

http://dx.doi.org/10.1016/j.margeo.2017.03.008
Received 8 November 2016; Received in revised form 1 March 2017; Accepted 17 March 2017
Available online 20 March 2017
0025-3227/

and its permanent halocline at depths between 40 and 80 m in the deeper central parts. As a consequence of the circulation pattern and the strong density stratification, vertical mixing is limited and water in the basin has a relatively long residence time of ~30 years (e.g. Wulff et al., 1990; Stigebrandt and Gustafsson, 2003). In combination with the excessive anthropogenic nutrient load over the past century, the aforementioned stratification has caused the Baltic Sea to become highly eutrophic (e.g. Gustafsson et al., 2012).

During the Holocene at least two other phases of widespread hypoxia have been recognized in the Baltic Sea (Zillén et al., 2008). The postglacial development of the Baltic Sea is characterized by an alternation between freshwater lake and brackish/marine conditions, which resulted from the complex interplay of the retreating ice sheet, isostatic rebound and eustatic sea level variations (e.g. Björck, 1995; Sohlenius et al., 1996; Andrén et al., 2011). Around 8 ka before present (BP) a permanent open connection with the North Sea was gradually established, leading to the modern brackish/marine conditions. The full transition from freshwater to brackish/marine conditions is observed in sedimentary records throughout the Baltic Sea. It is characterized by the widespread occurrence of laminated sediments (e.g. Zillén et al., 2008), a marked increase in sedimentary organic carbon content (C_{org}; e.g. Sohlenius et al., 2001), enrichments in molybdenum (Mo; e.g. Jilbert and Slomp, 2013; Dijkstra et al., 2016), the occurrence of the Fe-sulfide mineral greigite (Fe_3S_4; Lougheed et al., 2012; Reinholdsson et al., 2013) and the replacement of freshwater species of, for example, diatoms and dinoflagellates, by brackish/marine species (e.g. Andrén et al., 2000a; Brenner, 2005). Laminated, C_{org}, Mo and greigite rich sediments are deposited and preserved in hypoxic settings. The hypoxic interval from 8 to 4 ka BP (Zillén et al., 2008), coincides with the Holocene Thermal Maximum (HTM; ~9–5 ka BP; Snowball et al., 2004; Renssen et al., 2012) a period of relatively warmer climate. At the same time (~7–4 ka BP) the salinity in the Baltic Sea was at its maximum (e.g., Berglund, 1971; Gustafsson and Westman, 2002). The coupling of the warming and the establishment of a permanent halocline associated with marine water ingression are thought to have led to the oxygen depletion (Zillén et al., 2008). A second interval with widespread occurrence of laminated sediments, and a marked increase in sedimentary organic carbon content and Mo (e.g. Jilbert and Slomp, 2013; Dijkstra et al., 2016), indicative of hypoxic conditions, occurred between 2 and 0.8 ka BP (Zillén et al., 2008). This hypoxic interval also coincides with a period of regional climate warming: the Medieval Climate Anomaly (MCA; e.g. Esper et al., 2002). Furthermore, during this period the human population in the drainage area of the Baltic Sea rapidly increased, leading to large scale agricultural land use and soil nutrient release (Zillén and Conley, 2010). Together with regional climate warming, human activities thus may have driven the development of this second phase of widespread hypoxia (e.g. Carstensen et al., 2014b).

While the modern expansion of hypoxia has affected both the deep basins and the coastal zone of the Baltic Sea (Conley et al., 2011), relatively little is known about the bottom water redox conditions in the coastal zone of the Baltic Sea during the Holocene. On the one hand, the availability of nutrients is much higher in coastal waters, making these waters more vulnerable to eutrophication (e.g. Diaz and Rosenberg, 2008). On the other hand, coastal regions are often shallower, allowing better mixing of the water column, and therefore less stratification. The complex interplay of the factors leading to oxygen depletion in combination with the highly dynamic nature of the coastal zone makes it hard to reconstruct its past and predict its future redox state. Recently, Ning et al. (2016) showed that Gåsfjärden (a coastal site in southeast Sweden, that is presently intermittently hypoxic in late summer) was continually hypoxic before 3 ka BP. This suggests that hypoxia in the coastal zone was more persistent in the past, when three effects were occurring simultaneously: (1) the water depth at today's coastal sites was deeper due to local isostasy; (2) the Baltic Sea halocline was shallower due to more marine water ingression and higher salinity; (3) climate was warmer due to the HTM. Ning et al. (2016) note that the Gåsfjärden area was not hypoxic during the MCA period, which they attributed to the lack of a halocline and a shallower water depth resulting from isostatic rebound. These complex interactions illustrate that the drivers of hypoxia, such as changes in climate, nutrient input, local water depth and salinity, may be different in coastal and offshore areas.

Here we studied a Holocene sediment sequence from the south-eastern Danish coastal zone, located in the Little Belt (Site M0059), which was retrieved during Integrated Ocean Drilling Program (IODP) Expedition 347. The high sedimentation rate at this location (~50 m sediment deposition in the past ~8 ka; Andrén et al., 2015), which has been seasonally hypoxic since the 1970s (Karlson et al., 2002; Conley et al., 2007), and its proximity to the connection with the North Sea, make this site suitable for a detailed study of the freshwater lake to brackish/marine transition and the evolution of bottom water redox conditions throughout the Holocene. A variety of inorganic geochemical records, including bulk elemental data, as well as sulfur and iron speciation data, combined with a ^{14}C-based age model, shows that the transition to brackish/marine conditions was rapid and led to the development of persistent (seasonal) hypoxia.

2. Background

The Baltic Sea (Fig. 1a) was formed approximately 16 to 15 ka before present (BP) right after the last glaciation (e.g. Houmark-Nielsen and Kjaer, 2003). The retreating ice sheet left behind a large meltwater-filled ice lake, generally referred to as the Baltic Ice Lake (e.g. Björck, 1995). Around the onset of the Holocene (11.7 ka BP; Walker et al., 2009), the Baltic Ice Lake drained down to sea level through an outlet in south central Sweden (Jakobsson et al., 2007) and a new stage, the Yoldia Sea stage, began.

During the following ~350 years, freshwater from the melting ice sheet was still flowing out of the Baltic basin preventing any marine water to enter the basin. A small climate deterioration, the Preboreal oscillation, reduced the melt water flux and marine waters entered the basin around 11.3 ka BP. This brief and relatively weak brackish phase only lasted for a maximum of 350 years after which the Yoldia Sea stage ended with a freshwater phase (Andrén et al., 2002).

The shallowing outlets in the west forced the water level in the Baltic basin to rise and around 10.7 ka BP the next stage, known as the freshwater Ancylus Lake stage, began. For a period of ~500 years, the level of the Ancylus Lake continued to rise to as much as 10 m above sea level but at 10.2 ka BP the lake level fell again (Björck, 1995). This lake level drop occurred because the Ancylus Lake found an outlet in the southern Baltic basin through Mecklenburg Bay and Fehmarn Belt and out through the Great Belt to Kattegat (Fig. 1b) as a complex river system with river channels, levées, and lakes (Björck et al., 2008).

For the following period a couple of hundred years freshwater flowed out through this southern outlet, blocking seawater inflow. However, at 9.8 ka BP a first weak marine influence was recorded in both the Blekinge archipelago (Berglund et al., 2005) and in the Bornholm basin, and, although weaker, also in the Eastern Gotland basin (Andrén et al., 2000a, 2000b). This marks the start of a > 1000 years long transitional phase, the Initial Littorina Sea, characterized by a weak and fluctuating salinity, indicating that the Baltic basin was at level with the sea (Andrén et al., 2000b).

Between 8.5 and 8 ka BP the Öresund Strait (Fig. 1b) was flooded as a result of ongoing global sea level rise, establishing a permanent connection between the Baltic Sea and the North Sea through the Danish straits. This created the modern brackish/marine Baltic Sea, which is also referred to as the Littorina Sea (e.g.Andrén et al., 2011). This transition from a freshwater lake to the modern brackish/marine Littorina Sea is generally referred to as the Ancylus-Littorina transition (A/L transition; e.g. Sohlenius et al., 2001; Jilbert and Slomp, 2013). Since the onset of the Littorina Sea, ongoing glacio-isostatic rebound

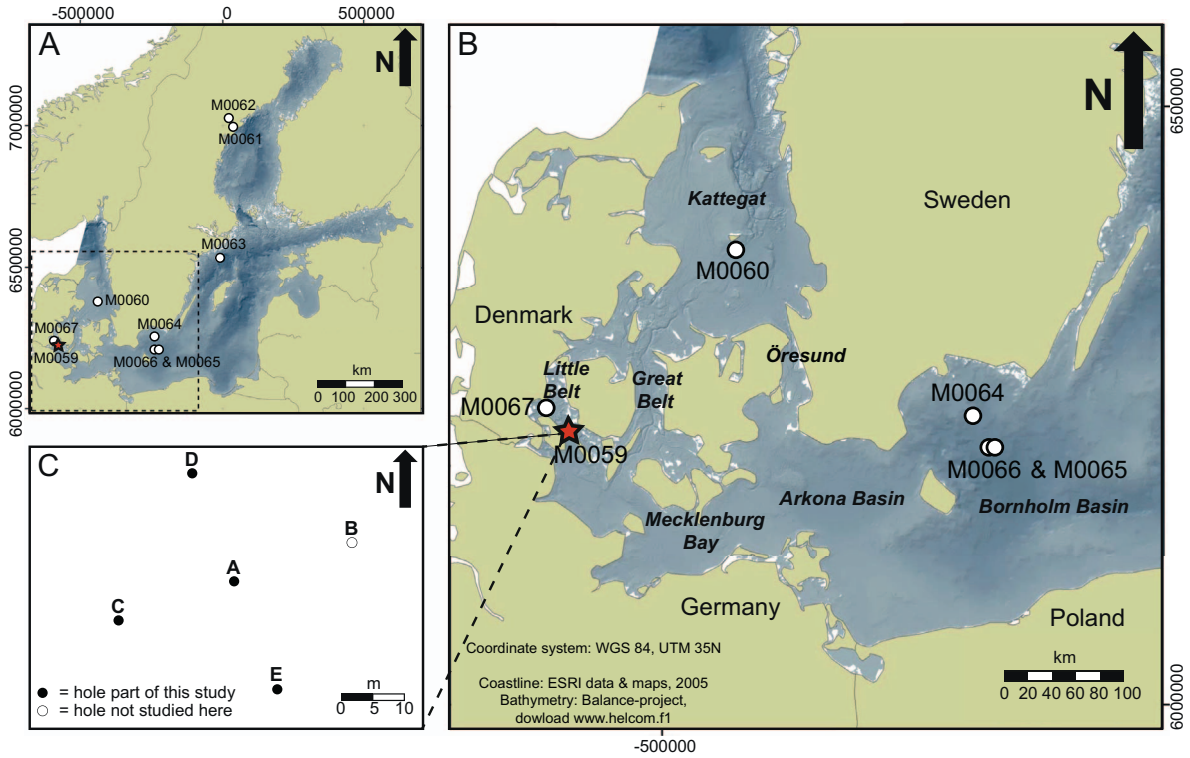

Fig. 1. Map of the Baltic Sea showing all the drill sites of IODP expedition 347 (A). Detailed map of the southwestern part of the Baltic Sea, with the different basins and straits indicated and the red star marking the location of the studied Site M0059 (B). Distribution of the different holes drilled at Site M0059 (C). Maps are modified from Andrén et al. (2015). (For interpretation of the references to colour in this figure legend, the reader is referred to the web version of this article.)

combined with (at some locations very fast) sedimentary infill has caused a shallowing of the Baltic Sea, reducing the average salinity of the sea by perhaps 6–8 (Widerlund and Andersson, 2011) and the total water volume by 47% (Meyer and Harff, 2005).

3. Materials and methods

3.1. Study site

At present, the Baltic Sea (Fig. 1a) is one of the largest brackish water bodies in the world, also ranking amongst the largest semi-enclosed basins globally. Its only connection with the open sea (North Sea) is through a series of straits, which are called (from northwest to southeast) the Skagerrak, the Kattegat and the Danish Straits (Little Belt, Great Belt and Öresund; Fig. 1b). The sediment samples used in this study were retrieved from coring Site M0059 (55°0.29′N, 10°6.49′E; 37.1 m water depth, with a tidal range < 10 cm), located in the Little Belt (Fig. 1a,b). Site M0059 was drilled with the *Greatship Manisha* in September and October 2013 as part of IODP Expedition 347. A detailed geophysical characterization of the sampling site, including seismic profiles, is provided in Andrèn et al. (2015). A total of five holes, A–E (Fig. 1c), were drilled, reaching a maximum depth in Hole B of 204.03 m below sea floor (mbsf). In order to couple the data of the different holes to each other, a composite depth scale (meters composite depth; mcd) was established, primarily based on the correlation of magnetic susceptibility between the different holes. In total, seven lithological units were identified (Andrén et al., 2015). Our study focuses on the uppermost three units (0–84 mcd). Unit III (53.62–~84 mcd) consists of greenish gray clay intercalated by centimeter-scale laminations consisting of well-sorted silt. A fining-upward trend was seen in Unit III based on an increase in the frequency of the laminations towards the base of the unit. A combination of lithology, biostratigraphy and onboard-geochemistry suggests that Unit III was deposited in a glacial meltwater lake (Andrén et al., 2015). Unit II (53.57–53.62 mcd) overlies Unit III, and consists of poorly sorted silty sand and some small clasts, suggesting an erosional unconformity and a much higher energy sedimentary environment, potentially marking a lowstand (Andrén et al., 2015). Unit I (0–53.57) is the uppermost lithological unit and can be separated into two subunits, Unit Ia (0–49.37 mcd) and Unit Ib (49.37–53.57 mcd). The base of Unit Ib consists of 10–15 cm of black laminated clays. The remainder of Unit Ib consists of greenish to gray, silty clay, intercalated by centimeter-scale pale green laminae. Abundant freshwater diatoms are indicative of a freshwater lake environment (Andrén et al., 2015). The top ~49 m, comprising Unit Ia, are composed of mostly homogeneous black to greenish black clay, with some millimetre-scale laminations and minor bioturbation. A combination of lithology, biostratigraphy and ship-board-geochemistry data indicate that Unit Ia was deposited in a brackish environment (Andrén et al., 2015).

3.2. Sediment samples

The sediment samples used in this study were taken from the cores retrieved from holes A, C, D and E. In the case of holes C and E, a set of samples was taken directly after core retrieval using cut-off syringes. These “offshore” samples were stored in aluminium sample bags, filled with nitrogen and sealed air-tight to prevent oxidation, which otherwise may cause artefacts in sediment chemical analyses, e.g. due to oxidation of Fe-sulfides (Burton et al., 2009; Kraal et al., 2009). For this study, 32 “offshore” samples for both holes C and E spread over Units I-III were processed. The remaining “onshore” samples were taken during the IODP Expedition 347 onshore sampling party at the Bremen Core Repository in January and February 2014. For holes A, C, D and E, 51, 108, 60 and 6 samples (respectively) were processed for the interval (~40–60 mcd) covering the main lithological transitions. Most of the “onshore” samples of Hole C are from core 17, Section 2. This core covers the transitions from Unit III to Unit II to Unit Ib and was sampled and processed on a centimeter-scale resolution between 30 and 135 cm.

To prevent sediment samples from oxidizing, the "offshore" sediment samples were freeze-dried, powdered and homogenized (using an agate mortar and pestle) in an oxygen-free atmosphere. Afterwards, a subsample was taken for the determination of organic carbon content (C_{org}) and total elemental concentrations. The "onshore" sediment samples were processed the same way, but under normal atmospheric conditions.

3.3. Organic carbon content

Approximately 0.3 g of freeze-dried and powdered sediment sample was weighed in centrifuge tubes, after which 7.5 ml of 1 M HCl was added to dissolve carbonates. After the bubbling of gas ceased, the tubes were closed and placed on a shaker. Four hours later, the acid was removed after centrifuging and fresh 1 M HCl was added to ensure complete decalcification. After a night on the shaker, the acid was removed after centrifuging and samples were washed with milliQ water to remove all acid. Subsequently, sediment samples were put in a stove at 60 °C until dry. To determine the weight loss by the removal of carbonates, the dried samples were weighed again. Finally, the samples were powdered and homogenized again using an agate mortar and pestle, after which 5–20 mg per sample was weighed in tinfoil cups. Measurements were performed using a Fisons Instruments NA 1500 NCS analyzer. Results were normalized to in-house standards, acetanilide, atropine and nicotinamide, and an internationally certified soil standard: IVA2. The certified value for IVA2 is 0.732 wt% C, our obtained mean value was 0.690 wt% C with a standard deviation of 0.016 wt% C. C_{org} was calculated upon correction for weight loss by decalcification. An average analytical uncertainty of 0.07 wt% was calculated based on duplicate analysis of sediment samples.

3.4. Total elemental composition

Approximately 125 mg of freeze-dried and powdered sediment sample was weighed in Teflon destruction vessels, after which the sediment was digested in 2.5 ml mixed acid (HNO_3:$HClO_4$; 2:3) and 2.5 ml 40% HF and left overnight on a hotplate at 90 °C. The following day the lids were removed and the extracts were heated to 140 °C in order to evaporate the acids. Afterwards, the residues were dissolved in 25 ml 4.5% HNO_3 and left overnight on a hotplate at 90 °C. The resulting extracts, with a dilution of ~200–250, were measured by Inductively Coupled Plasma-Optical Emission Spectrometry (ICP-OES; SPECTRO ARCOS), to determine sedimentary elemental compositions. The reference material ISE-921 was used to determine accuracy and precision. The accuracy (recovery) was generally between 95 and 105% and the relative errors were < 5% for all reported elements. The average analytical uncertainty based on s duplicates and triplicates was 4% for calcium (Ca), 3% for iron (Fe), 5% for manganese (Mn), 8% for molybdenum (Mo), 3% for phosphorus (P), 30% for lead (Pb) and 7% for S. The calcium carbonate content ($CaCO_3$ wt%), was calculated based on the Ca content measured by ICP-OES.

3.5. Iron speciation

Iron was sequentially extracted following the method of Poulton and Canfield (2005). Between 50 and 100 mg of sediment sample was weighed in centrifuge tubes in an argon-gas-filled glovebox. To extract carbonate-associated Fe (Fe_{carb}), 10 ml of 1 M sodium acetate brought to pH 4.5 with acetic acid was added to the sediment sample in the glovebox. After shaking for 24 h and centrifugation, the supernatant was removed and filtered over a 0.45 µm filter and stored at 4 °C until measurement. Subsequently, 10 ml 1 M hydroxylamine-HCl in 25% v/v acetic acid was added and the tube was placed on a shaker table for 48 h to extract easily reducible (amorphous) Fe-oxides (Fe_{ox1}), e.g. ferryhydrite. During this extraction step part of the iron monosulfides (FeS) might dissolve as well (Egger et al., 2015). After removal, filtration and storage of the supernatant, 10 ml sodium dithionite solution buffered to pH 4.8 with 0.35 M acetic acid/0.2 M sodium citrate was added to the remaining sediment and the tube was placed on the shaker table for 2 h to extract the reducible, crystalline Fe-oxides (Fe_{ox2}), including goethite and hematite. Supernatants were again removed, filtered and stored, after which 10 ml of 0.2 M ammonium oxalate/0.17 M oxalic acid solution was added and put on the shaker table for 2 h to extract magnetite (Fe_{mag}). The Fe content in all extracts was determined colorimetrically using the 1,10-phenanthroline method (APHA, 2005). Average analytical uncertainty, based on duplicates, was ~10% for all fractions.

3.6. Sulfur speciation

The Burton et al. (2008) method was used to determine the amount of acid-volatile sulfur (AVS, assumed to represent iron FeS) and chromium-reducible sulfur (CRS, assumed to represent pyrite (FeS_2)). About 0.5 g of sediment sample was weighed into centrifuge tubes in an argon-gas-filled glovebox, after which a smaller centrifuge tube, containing 7 ml of alkaline zinc acetate solution, was placed in the centrifuge tube holding the sediment sample. To determine the amount of AVS, 10 ml 6 M HCl and 2 ml 0.1 M ascorbic acid were added to the sediment, after which samples where put upright on a shaker overnight. The produced sulfide gas was then trapped in the alkaline zinc acetate solution, forming a precipitate of zinc sulfide. After disposal of the supernatant and replacement of the trap, the amount of CRS was determined by addition of 10 ml chromium(II)chloride. The samples were left on a shaker table for 48 h, and the produced sulfide was trapped in the alkaline zinc acetate solution again. The amount of sulfur in the zinc sulfide precipitates was determined by iodometric titration (APHA, 2005). Average analytical uncertainty, based on duplicates, was ~2 µmol/g and ~15 µmol/g for AVS and CRS respectively.

3.7. Core chronology

The age-depth model for the upper 49 mcd of Site M0059 (Fig. 2) is based on radiocarbon dating of bivalve fragments and intact bivalve specimens (*Abra alba*, *Macoma balthica*; Table 1). A lack of organic

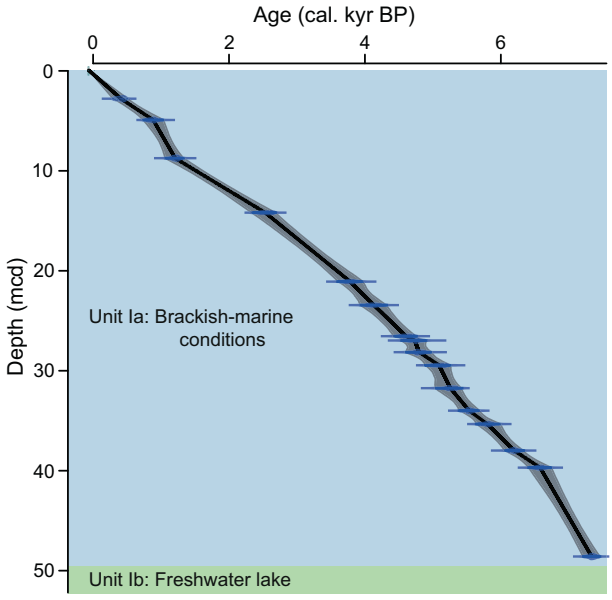

Fig. 2. Age model for Site M0059. In blue are the ^{14}C ages with the blue bars representing their uncertainty. The black line gives the age-depth model based on linear regression. The gray shaded area marks the 95% (2σ) confidence interval of the age-depth model. (For interpretation of the references to colour in this figure legend, the reader is referred to the web version of this article.)

Table 1
Sample laboratory IDs, sample depths, material and 14C dates used to construct the age-depth model for Site M0059 (Fig. 2). Complete sample codes are provided in Supplementary data.

Laboratory ID	Composite depth (m)	Material dated	^{14}C Age	Error	Calibrated age, (2σ)	Min. (2σ)	Max. (2σ)
LuS11289	2,84	Molluscs, *Abra alba*	700	35	405	297	513
LuS11476	4,97	Molluscs, *Abra alba*	1265	35	899	755	1043
LuS11291	8,79	Molluscs, *Abra alba*	1585	35	1213	1083	1348
LuS11292	14,24	Molluscs, *Macoma balthica*	2740	40	2556	2383	2729
LuS11477	21,14	Molluscs, *Macoma balthica*	3780	35	3829	3645	4013
LuS11295	23,49	Molluscs, *Macoma balthica*	4035	40	4187	3993	4381
LuS11479	26,60	Molluscs, *Macoma balthica*	4395	40	4664	4500	4827
LuS11297	27,03	Molluscs, *Macoma balthica*	4500	40	4785	4598	4971
LuS11480	28,20	Molluscs, *Macoma balthica*	4540	40	4845	4654	5036
LuS11300	29,51	Molluscs, *Macoma balthica*	4780	40	5147	4949	5345
LuS11481	31,80	Molluscs, *Macoma balthica*	4890	40	5313	5118	5507
LuS11482	34,05	Molluscs, *Abra alba*	5155	40	5603	5457	5748
LuS11301	35,39	Molluscs, *Abra alba*	5415	40	5885	5713	6057
LuS11483	38,04	Molluscs, *Abra alba*	5770	40	6289	6152	6426
LuS11303	39,75	Molluscs, *Macoma balthica*	6130	40	6662	6494	6829
LuS11304	48,64	Mollusc fragments, bivalve	6845	45	7437	7311	7562

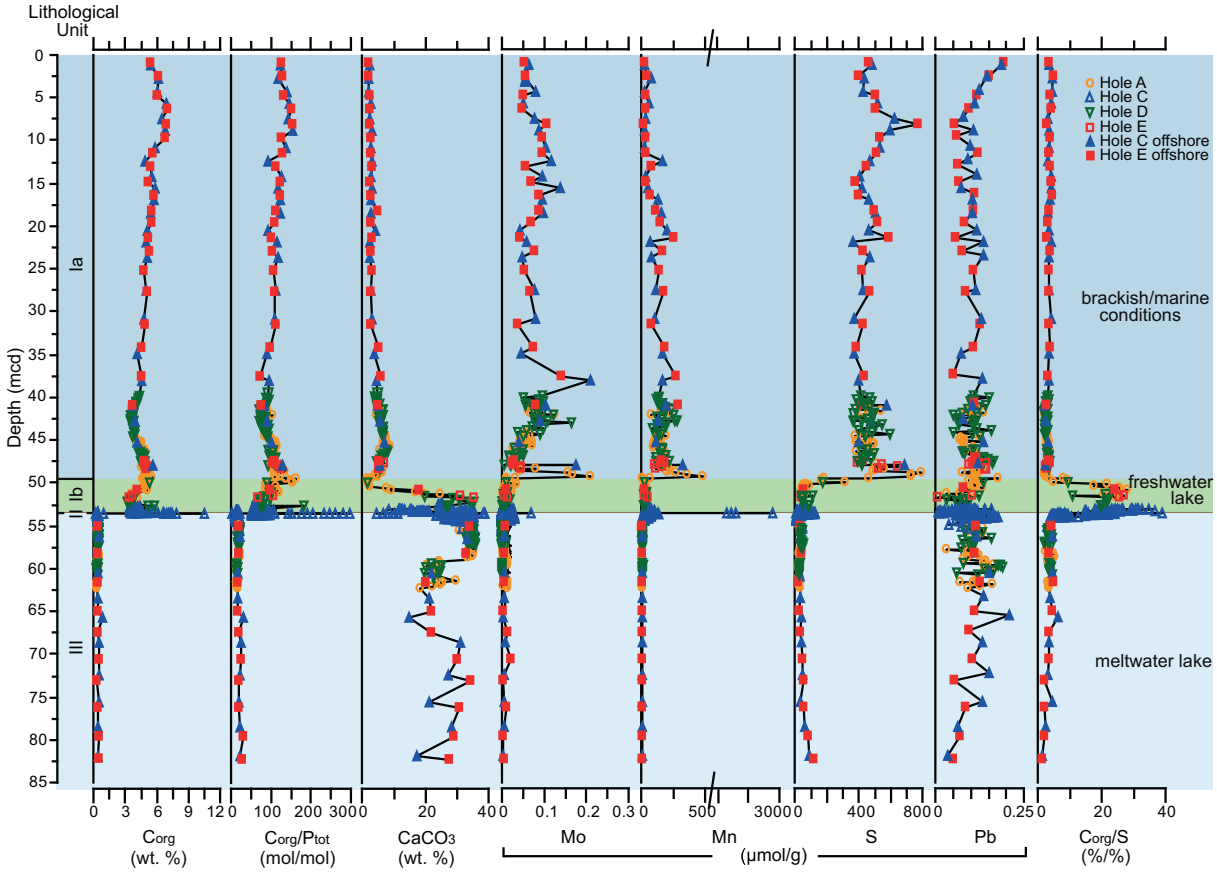

Fig. 3. Profiles of, C_{org}, C_{org}/P_{tot}, $CaCO_3$, Mo, Mn, S, Pb and C_{org}/S for Site M0059 plotted against depth. The calcium carbonate content ($CaCO_3$ wt%), was calculated based on the Ca content. Lithology is shown on the left, while on the right side the corresponding environment is indicated.

matter (Fig. 3) and in-situ carbonate fossil material precludes radiocarbon dating in the deeper intervals of the record. Dates used in the age model are limited to bivalve material obtained from the Site M0059 composite stratigraphic splice (additional ^{14}C samples from foraminifera and samples outside the splice were omitted but are shown in the Supplemental table), because differential compaction and expansion between adjacent holes can introduce significant offset when assigning composite depths (mcd) to off-splice intervals (Obrochta et al., 2014), and because different organisms show different ^{14}C–age offsets. However, one sample outside the splice was included (M0059E-3H-2W, 32–33 cm (8.79–8.80 mcd)) because omitting this samples would result in a long section without age control. Additionally, two dates at M0059D-2H-2 15–17 cm (3.45–3.47 mcd) and M0059D-12H-2 33–34 cm (36.63–36.64 mcd), which would produce large age reversals, were excluded. The sediment surface was assumed to be modern (i.e. 2013, the year of coring). ^{14}C determinations via accelerator mass spectrometry (AMS) were performed at the Radiocarbon Dating Laboratory, Lund University, Sweden.

The age-depth modeling was performed using the age-modeling software CLAM version 2.2 (Blaauw, 2010) with 2000 iterations using the Marine13 calibration dataset (Reimer et al., 2013) and a deviation (ΔR) of − 90 ± 53 from the Marine13 reservoir age. The chosen ΔR is

Table 2
Average (avg.) and maximum (max.) values per lithological unit for C_{org}, C_{org}/P_{tot}, Mo, $CaCO_3$, Mn, S and C_{org}/S.

Lithological unit	C_{org} (wt%)		C_{org}/P_{tot} (mol/mol)		$CaCO_3$ (wt%)		Mo (μmol/g)		Mn (μmol/g)		S (μmol/g)		C_{org}/S (%/%)	
	Avg.	Max.	Avg.	Max.	Avg.	Max.	Avg.	Max.	Avg.	Max.	Avg.	Max.	Avg.	Max.
Unit Ia	4.8	7.0	105	155	5	9	0.074	0.211	144	484	473	791	3	5
Unit Ib	4.6	10.5	103	298	21	39	0.005	0.069	48	111	75	316	22	36
Unit II	0.4	1.0	9	23	8	11	0.006	0.028	1477	2780	12	35	16	39
Unit III	0.4	0.9	17	31	30	36	0.005	0.031	21	153	32	121	5	20

a mean based on the values for ΔR for suspension and deposit feeders in three study sites relatively close to Site M0059, as reported in the Marine Reservoir Correction Database (http://calib.org/marine/), MapNo 1692, 1693 (Lougheed et al., 2013) and MapNo 93 (Heier-Nielsen et al., 1995). All subsequent ages discussed refer to calibrated ages in years before 1950 CE (cal. yr. BP).

The mean sedimentation rate in the upper 49 mcd (Unit Ia) of the studied record is 0.66 cm/yr, and sedimentation is generally steady, with no evidence of abrupt changes in sedimentation rate (Fig. 2).

4. Results

4.1. Unit III – glacial meltwater lake phase (53.62–~84 mcd)

Unit III is characterized by consistently low C_{org} concentrations (< 0.5 wt%) and C_{org}/P_{tot} ratios (< 30; Fig. 3; Table 2). Concentrations of Mo are very low. Mn concentrations are also low, averaging ~20 μmol/g. Sulfur concentrations are slightly elevated at the base of the studied interval, at ~100 μmol/g, but gradually decrease to values below 20 μmol/g at the top of Unit III. In combination with the stable C_{org} concentrations, this results in increasing C_{org}/S ratios towards the top of Unit III (Fig. 3; Table 2). $CaCO_3$ contents vary from ~20 to 35%. Most of the extractable Fe in Unit III consists of Fe-oxides, with an average concentration of ~100 μmol/g. Magnetite concentrations are relatively high (~20 μmol/g), while Fe carbonate concentrations are relatively low (30 μmol/g; Fig. 6) and FeS is nearly absent (Fig. 6; Table 3).

4.2. Unit II – lowstand phase (53.57–53.62 mcd)

Unit II is characterized by the lowest values of C_{org}, C_{org}/P_{tot}, Fe and S in the entire record, with the latter resulting in a high C_{org}/S ratio at the onset of Unit II (Figs. 3 and 4). In contrast, Mn concentrations are very high with values up to 2800 μmol/g, or ~15 wt% (8 wt% on avg.; Figs. 3 and 4). Again, Mo concentrations are negligible. The $CaCO_3$ concentration strongly decreases at the onset of Unit II to values of ~10 wt% (Figs. 3 and 4). None of the available "offshore" samples were from Unit II, hence there are no sequential extraction data for this unit.

4.3. Unit Ib – freshwater lake phase (49.37–53.57 mcd)

The onset of Unit Ib is characterized by the highest C_{org} and C_{org}/P_{tot} values for the studied interval, with an average C_{org} concentration of 7.5 wt% for the first 10 cm and a maximum well above 10 wt%. For the same interval, C_{org}/P_{tot} values average around 200, with maxima up to 300 (Figs. 3 and 5). After this first C_{org}-rich layer, values decrease to around 4 wt% and C_{org}/P_{tot} values drop to ~100. From 52 mcd onwards both C_{org} and C_{org}/P_{tot} start to increase again, reaching maximum values of 5 wt% and 150 towards the end of Unit Ib (Figs. 3 and 5). The sediments in the first centimeters of Unit Ib are somewhat enriched in Mo, but in the remainder of Unit Ib Mo concentrations are very low (Figs. 3 and 5). Concentrations of Mn return to low, pre-Unit II values, averaging around 50 μmol/g (Fig. 3; Table 2). At the onset, S concentrations are elevated, up to 140 μmol/g. In the following ~20 cm S concentrations gradually decrease to 50 μmol/g, after which they increase again towards the transition to Unit Ia (Figs. 3 and 5). Despite the somewhat elevated S concentrations at the onset and at the termination, Unit Ib is characterized by high C_{org}/S values, averaging well above 20, resulting from the relatively high C_{org} concentrations (Figs. 3 and 5; Table 2). Unfortunately only one sample was available for the sequential extractions of Fe and S for Unit Ib. The results for this sample (50.73 mcd) suggest that Fe-oxides remain the dominant form of extractable iron and that the concentration of Fe-sulfides remains relatively low (Fig. 6; Table 3).

4.4. Unit Ia – brackish/marine phase (0–49.37 mcd)

At the onset of Unit Ia, C_{org} concentrations are around 5 wt%, while C_{org}/P_{tot} values are around 150. Right after the onset of Unit Ia around 40 mcd, C_{org} and C_{org}/P_{tot} values gradually decrease to ~3.5 wt% and 80, respectively (Figs. 3 and 5). Above 40 mcd, C_{org} concentrations and C_{org}/P_{tot} values gradually rise, again to ~5.5 wt% and 130 at the top of the core. Superimposed on this gradual rise there is a maximum in C_{org} and C_{org}/P_{tot} between 10 and 5 mcd, with C_{org} concentrations as high as 7% and C_{org}/P_{tot} up to ~150 (Figs. 3 and 5). The concentration of $CaCO_3$ increases to ~5–8% at the onset of Unit Ia and gradually decreases towards the top of the record (Figs. 3 and 5). Right after the onset of Unit Ia, the concentration of Mo reaches a maximum (~0.2 μmol/g; Figs. 3 and 5). After this distinct maximum, Mo concentrations fall to values around 0.03 μmol/g and then gradually increase again, reaching a second maximum of similar magnitude around 38 mcd. For the remainder of the record Mo concentrations generally vary between 0.05 and 0.1 μmol/g (Figs. 3 and 5). The Mn record shows trends comparable with Mo, with a maximum concentration right after the onset of Unit Ia (~500 μmol/g; Figs. 3 and 5; Table 2). After a sharp decrease, Mn concentrations generally vary between 150 and 200 μmol/g up to a depth of 20 mcd, after which they drop back to concentrations comparable with those measured for Unit

Table 3
Average (avg.) and maximum (max.) values per lithological unit for total Fe, the different extracted Fe fractions and Fe-sulfides.

Lithological unit	Fe_{total} (μmol)		Fe_{oxides} (μmol)		Fe_{carb} (μmol)		Fe_{mag} (μmol)		Fe_{AVS} - FeS (μmol)		Fe_{CRS} - FeS_2 (μmol)	
	Avg.	Max.	Avg.	Max.	Avg.	Max.	Avg.	Max.	Avg.	Max.	Avg.	Max.
Unit Ia	677	831	33	48	108	195	11	18	30	96	120	255
Unit Ib	492	1082	106	106	59	59	17	17	2	2	6	6
Unit II	342	474	–	–	–	–	–	–	–	–	–	–
Unit III	632	1284	85	150	30	58	21	33	1	3	20	53

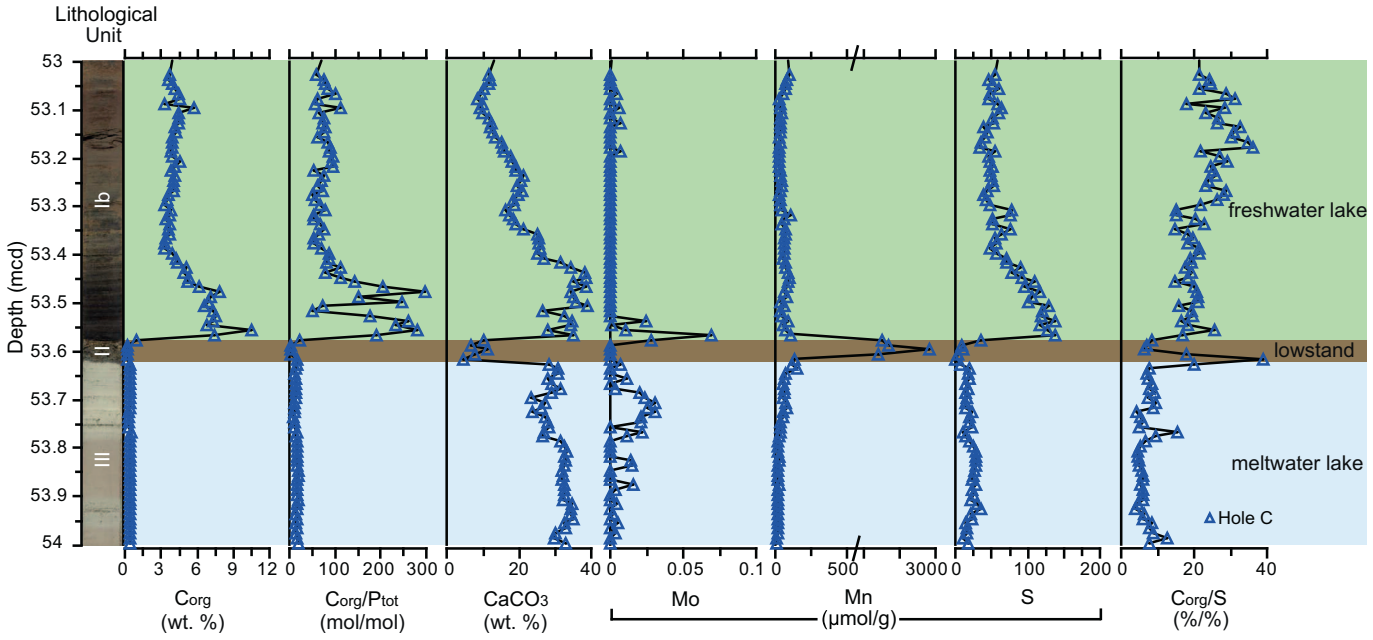

Fig. 4. Core photograph of the studied interval (Site M0059, hole C, core 17-H, Section 2 from 30 to 130 cm) between 53 and 54 mcd, comprising the transition from Unit III to Unit II and the transition from Unit II to Unit Ib, with C_{org}, C_{org}/P_{tot}, $CaCO_3$, Mo, Mn, S, and C_{org}/S plotted next to it. Note that each data point represents a 1 cm slice of sediment.

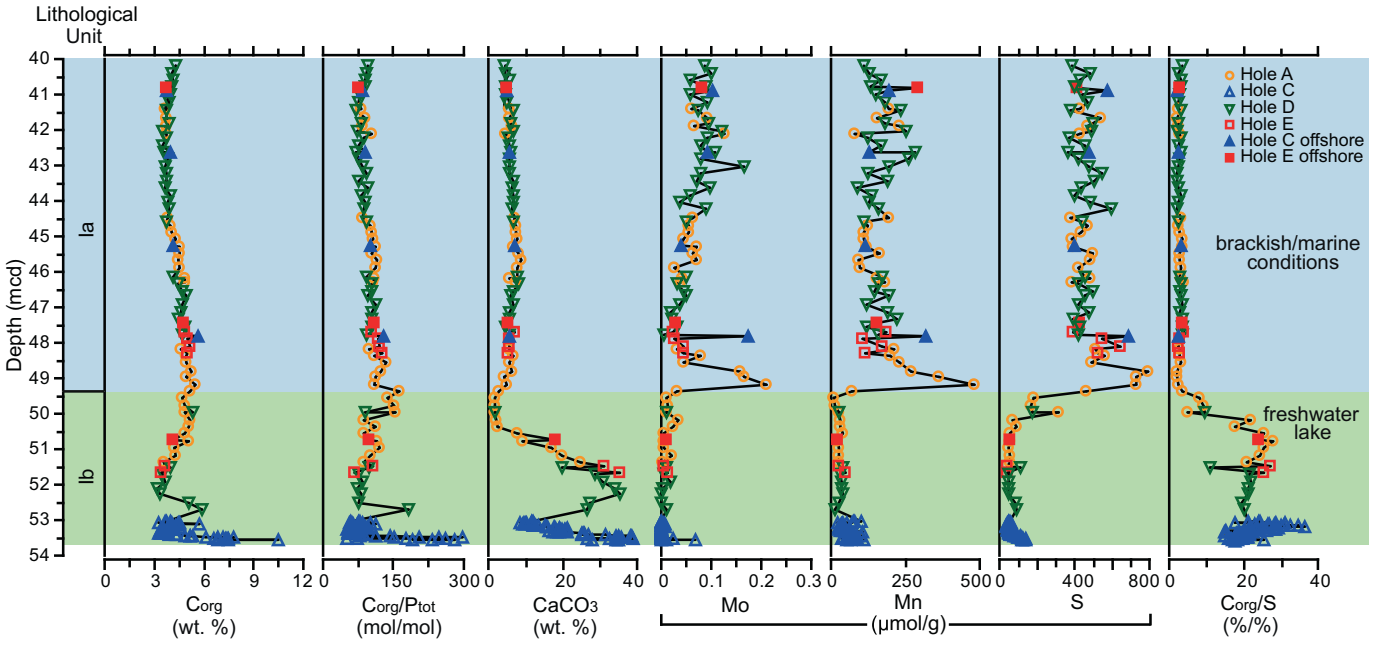

Fig. 5. Profiles of, C_{org}, C_{org}/P_{tot}, $CaCO_3$, Mo, Mn, S, and C_{org}/S around the transition from the freshwater lake to the brackish-marine Littorina Sea for Site M0059 plotted against depth. The calcium carbonate content ($CaCO_3$ wt%), was calculated based on the Ca content. Lithology is shown on the left, while on the right side the corresponding environment is indicated.

Ib and Unit III (Figs. 3 and 5). Sulfur concentrations already showed an increasing trend towards the top of Unit Ib, this increase continues at the onset of Unit Ia, reaching maximum values close to 800 µmol/g around 49 mcd (Figs. 3 and 5). Subsequently S concentrations drop again and remain relatively stable for the remainder of the record (average ~ 450 µmol/g), with the exception of two maxima around 20 mcd (~600 µmol/g) and 8 mcd (~750 µmol/g; Figs. 3 and 5), as a consequence of relatively high S concentrations C_{org}/S ratios are much lower in comparison with Unit Ib, averaging around 3 (Figs. 3 and 5; Table 2). Lead concentrations vary throughout the record but show a consistent increase from 8 mcd upwards (Figs. 3 and 5). In contrast with the underlying units, Fe carbonate represent the largest fraction of the extractable Fe in Unit Ia, generally averaging around 130 µmol/g, with the exception of a distinct minimum (~40 µmol/g) between 12 and 7 mcd. Fe-oxides and magnetite represent a relatively minor part of the extractable Fe, averaging around 35 µmol/g and 10 µmol/g, respectively. Unit Ia is characterized by high concentrations of Fe-sulfides, dominated by FeS_2. Concentrations of FeS_2 are generally around 100 µmol/g, with distinct maxima at the onset of Unit 1a and around 40, 20 and 10 mcd (Fig. 6, Table 3).

5. Discussion

5.1. Glacial meltwater lake: an oligotrophic, oxic environment

The glacial lake sediments of Unit III are low in S, indicating sulfate-

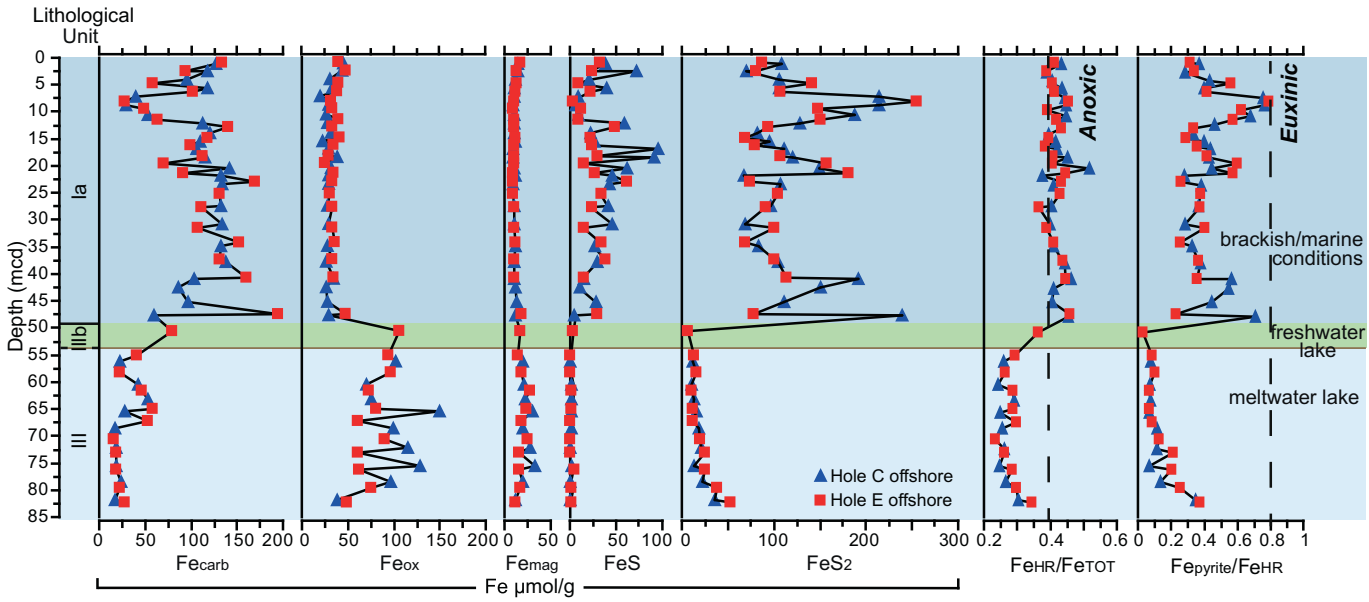

Fig. 6. Profiles of solid phase Fe fractions and for Site M0059 plotted against depth. The fractions are Fe-carbonate (Fe_{carb}), Fe oxides (Fe_{ox}), magnetite (Fe-mag), iron monosulfides (FeS) and pyrite (FeS_2). The two right panels show the sum of the highly reactive iron minerals (Fe_{HR}) divided by total sedimentary Fe (Fe_{TOT}) (A). The dashed line (0.38) indicates the value above which deposition took place in anoxic bottom waters (e.g. Poulton and Canfield, 2011). Profile of Fe in the form of pyrite (Fe_{pyrite}) divided by Fe_{HR} (B). The dashed line (0.8) indicates the value above which deposition took place under euxinic conditions (Anderson and Raiswell, 2004). Lithology is shown on the left, while on the right side the corresponding environment is indicated.

poor overlying waters, i.e. a freshwater environment (e.g. Berner and Raiswell, 1984). The high $CaCO_3$ content is due to the glacial reworking of the extensive regional Cretaceous chalk bedrock (Andrén et al., 2015). The low sedimentary C_{org} content is the result of several factors, including the low organic matter flux to the seafloor as a result of a very low primary production in such a glacial lake setting, the redox state of the water column and surface sediments, and potentially large dilution with inorganic sediment (e.g. Reed et al., 2011), such as may occur during rapid sedimentation in a proglacial lake. The observed centimeter-scale laminations, i.e. varves, consisting of well-sorted silt, intercalating the generally greenish gray clay, are the result of such rapid sedimentation events. The low C_{org} and C_{org}/P_{tot} values (Fig. 3) suggest that Unit III was deposited in a well-oxygenated and low productivity environment (e.g., Algeo and Ingall, 2007). Besides C_{org} and C_{org}/P_{tot}, sedimentary enrichment in Mo is a widely used proxy to determine the degree of oxygen depletion in marine sediments, with increasing sedimentary Mo concentrations pointing to more reducing conditions (e.g. Emerson and Huested, 1991; Helz et al., 1996; Scott and Lyons, 2012). This proxy has also successfully been applied in lakes (e.g. Schaller et al., 1997; Chappaz et al., 2008). The absence of Mo enrichments and the relatively high concentration of Fe-oxides in Unit III (Figs. 3 and 6) therefore provide additional evidence for a well-oxygenated water column during the deposition of Unit III. Unfortunately, there are no reliable age estimates available for Unit III, making it impossible to determine whether Unit III represents the Baltic Ice Lake or an earlier glacial lake phase with similar conditions.

5.2. Drainage of a proglacial lake: erosion and deposition of sand

The sharp and irregular contact between Unit II and Unit III (Fig. 4), most likely represents an erosional unconformity (Andrén et al., 2015). Despite the marked lithological change, Unit II shows similar, low values for C_{org}, C_{org}/P_{tot}, Mo and S, as observed for Unit III. However, particularly the Mn concentrations show a large increase (Fig. 4). These high Mn concentrations in combination with the coarse clasts (up to pebble-size; Andrén et al., 2015), suggest an allochthonous origin. A possible source of the Mn-rich sediments is the Baltic Shield. The waxing and waning of glaciers led to the grinding up and dispersion of bedrock fragments across Scandinavia and beyond (e.g. Melkerud et al., 2000). Because large parts of the central and northern Baltic Shield are rich in mineral deposits, including Mn-ores (e.g.; Frietsch et al., 1979; Rickard, 1979), this scenario could also explain the high Mn concentrations. One possible explanation for the erosive contact between Unit III and Unit II could be that it resulted from a sudden lowering of the water level and subaerial exposure of the site, for example resulting from one of the drainage events of the Baltic Ice Lake (e.g. Björck and Digerfeldt, 1989; Jakobsson et al., 2007; Bennike and Jensen, 2013). Afterwards, when the region was flooded again, an initially high-energetic depositional system prevailed, leading to the deposition of the coarse sandy layer. An alternative explanation for the high Mn concentrations in Unit II could be the precipitation of Mn carbonates from the pore waters in this coarse grained sediment.

5.3. Ancylus Lake stage: a eutrophic, oxic freshwater environment

The generally low S and high C_{org}/S values for Unit Ib (Fig. 3) are indicative of freshwater conditions (Berner and Raiswell, 1984). All samples plot far below the line that represents normal marine (non-euxinic) modern sediments (Fig. 7; Berner and Raiswell, 1983). In other regions of the Baltic Sea, the C_{org} content of sediments from this time period (the Ancylus Lake stage) is generally low. This suggests that productivity was relatively low during this stage, which can be attributed to the combined effect of the nutrient-poor meltwater input and the lack of topsoil development in the recently deglaciated drainage area (Andrén et al., 2011). However, our record shows high C_{org} values for the entire freshwater lake phase, making it distinctly different from other Baltic records. Therefore, we infer that there must have been large regional differences in nutrient supply and, subsequently, in productivity. The Little Belt area received relatively nutrient-rich riverine input from Denmark and Germany instead of nutrient-poor meltwater and riverine water still present in areas further north, which had relatively organic-poor sediment immediately after the recent deglaciation (e.g. Andrén et al., 2011). The enrichments in C_{org}, Mo and S and high C_{org}/P_{tot} values in the deepest, laminated sediments of Unit Ib (Fig. 4) suggest that this input may have led to a short period of low oxygen conditions (e.g. Algeo and Ingall, 2007;

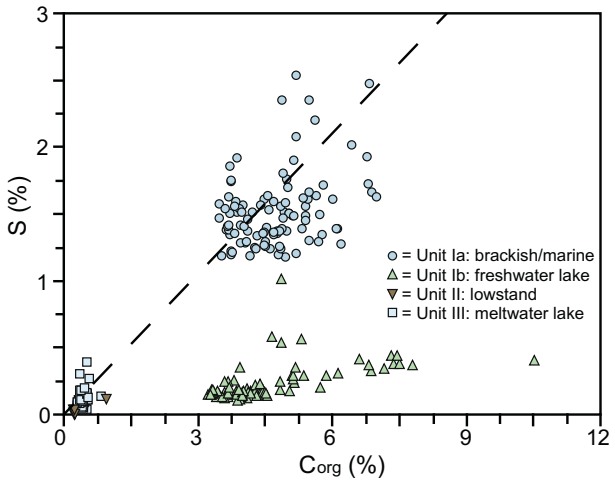

Fig. 7. Cross plot of total sedimentary S versus C_{org} for the different studied lithological units of Site M0059. The dashed line represents C_{org} vs. wt% pyrite for normal marine (non-euxinic) modern sediments by Berner and Raiswell (1983).

Scott and Lyons, 2012). Our results also support the work by Jensen et al., 1999 and Bennike and Jensen, 2011, who suggested that a local lake existed in the Little Belt area at this time that may not have been connected to the coeval Ancylus Lake, which occupied the central part of the Baltic Sea. Towards the top of the unit, a gradual increase in C_{org} is recognized (Fig. 3). Such an increase was recognized in sedimentary records from other sites as well (e.g. Andrén et al., 2000a, 2000b; Böttcher and Lepland, 2000; Sohlenius et al., 2001; Dijkstra et al., 2016). We suggest that, besides enhanced terrestrial input of C_{org}, climatic warming leading into the HTM (e.g. Snowball et al., 2004; Renssen et al., 2012) may have been driving this Baltic Sea-wide trend, enhancing primary productivity and decreasing the solubility of oxygen in the surface waters of the Baltic, thereby also preconditioning the Baltic Sea for widespread hypoxia (e.g. Zillén et al., 2008; Jilbert and Slomp, 2013). Despite the relatively high C_{org}, no enrichments in Mo are observed, and the only available sample from this freshwater lake phase for Fe and S extractions shows relatively high concentrations of Fe-oxides and low concentrations of Fe-sulfides, indicating well-oxygenated (bottom) water conditions. We attribute the somewhat elevated S concentrations in the upper part of the freshwater lake sediments to downward sulfurization (Jørgensen et al., 2004).

5.4. *Littorina Sea stage: a brackish/marine, seasonally hypoxic environment*

The rapid increase in S and decrease in C_{org}/S values around 49 mcd (Fig. 3) indicate a switch from a freshwater environment to brackish/marine conditions (Berner and Raiswell, 1984), as at the Ancylus-Littorina transition (A/L transition; e.g. Sohlenius et al., 2001; Jilbert and Slomp, 2013), but with a local freshwater lake potentially present at this site during the Baltic Sea's Ancylus stage (Jensen et al., 1999; Bennike and Jensen, 2011). Furthermore, all samples of Unit Ia plot around the line that represents normal marine (non-euxinic) modern sediments (Fig. 7; Berner and Raiswell, 1983), confirming more marine, presumably brackish conditions, in agreement with the foraminifera and diatom assemblages encountered in this unit (Andrén et al., 2015).

The sudden establishment of a halocline at the A/L transition is characterized as a major lithological change in sedimentary archives throughout the Baltic Sea (Andrén et al., 2011), with many basins (particularly the deeper basins) showing a switch from bioturbated clays to laminated sediments (e.g. Zillén et al., 2008), suggesting decreases in benthic macrofauna resulting from hypoxia (e.g. Ekdale and Mason, 1988). Sediments after the A/L transition are generally characterized by a marked increase in $C_{org,}$ (e.g. Jilbert and Slomp, 2013; Dijkstra et al., 2016). Despite a broad maximum in C_{org} at the A/L transition, a sharp C_{org} increase is absent in the Little Belt. We attribute this absence to the already elevated C_{org} during the preceding freshwater lake phase. The gradual rise in C_{org} during the brackish/marine Littorina Sea in the Little Belt (Fig. 3) can be linked to a gradual decrease of water depth as a result of sedimentary infill of the site (due to continuously high sedimentation rates of ~0.66 cm/yr (Fig. 2)). Assuming a generally constant nutrient input, the shrinking water column will have become more nutrient rich, supporting a gradual increase in productivity and the observed gradual increase in C_{org} (e.g. Hutchinson, 1973).

High Mo concentrations in sediments from the deeper parts of the Baltic Sea (up to 3 μmol/g; e.g. Jilbert et al., 2015; Dijkstra et al., 2016), indicate that bottom water conditions may even have become euxinic, i.e. suggest that there was free sulfide present (e.g. Scott and Lyons, 2012) right after the A/L transition. The sudden deposition of Mo in the Little Belt after the A/L transition also suggests oxygen depletion, but the concentrations of Mo are mostly below 0.2 μmol/g. These values are within the range (< 0.26 μmol/g) that are thought to indicate that sulfide was restricted to pore waters (Scott and Lyons, 2012). The continuous sequestration of Mo nevertheless suggests (seasonal) hypoxia occurred continuously after the A/L transition.

The presence of hypoxia is further confirmed by elevated concentrations of highly reactive iron minerals, i.e. Fe-carbonates (e.g. siderite and ankerite), Fe-oxides (e.g. ferrihydrite, and goethite), magnetite and pyrite, over total sedimentary Fe ($Fe_{HR}/Fe_{TOT,}$ Fig. 6; e.g. Raiswell and Canfield, 1998; Poulton and Raiswell, 2002). Based on an evaluation of ancient sediments, a Fe_{HR}/Fe_{TOT} value of 0.38 was determined to represent an extreme upper value for oxic conditions before the transition to hypoxia (Poulton and Canfield, 2011). The Fe_{HR}/Fe_{TOT} value for the Little Belt sediments after the A/L transition is almost continuously above 0.38, and thus falls within the range for anoxic bottom waters (Poulton and Canfield, 2011). However, based on the low Mo values, we conclude that extensive anoxia in the water column is unlikely. The pyrite over Fe_{HR} ratio (Fe_{pyrite}/Fe_{HR}, Fig. 6), which can be used to distinguish ferruginous from euxinic conditions, shows values below 0.8, indicative of non-euxinic deposition (e.g. Anderson and Raiswell, 2004), in agreement with the Mo concentrations. Besides the abrupt onset in deposition of Mo, Mn is also sequestered after the A/L transition. Sedimentary enrichment of Mn after the A/L transition was previously observed for records throughout the Baltic Sea and attributed to the mobilization of Mn during hypoxic conditions after which it would be recaptured during oxic phases, and then permanently buried as Mn-carbonates (e.g. Huckriede and Meischner, 1996; Sohlenius et al., 1996; Neumann et al., 1997; Lenz et al., 2015). The absence of Mn in the upper part of the record suggests either a more limited Mn oxide input (required for subsequent formation of Mn-carbonates) or less efficient conversion to Mn carbonates. Besides the absence of Mn, the upper part of the Little Belt record is characterized by low Fe_{carb} and a maximum in FeS_2 (Fig. 6), suggesting that a larger proportion of the Fe was transformed to Fe-sulfides. The absence of high Mo concentrations, however, indicates that most of the Fe must have been transformed to Fe-sulfides at the sediment-water interface or in the sediment itself rather than in the water column.

When our geochemical dataset is plotted against the age model (Fig. 8), it shows that the hypoxic intervals in the Baltic Sea that largely coincide with the HTM and MCA (Zillén et al., 2008) are much less pronounced in the Little Belt than at deep basin sites (e.g. Jilbert and Slomp, 2013; Lenz et al., 2015; Jilbert et al., 2015; Dijkstra et al., 2016). The early stages of the HTM do, however, coincide with maxima in Mo and a maximum in C_{org} at the A/L transition (Figs. 3 and 8). The MCA interval, which can be approximately dated based on the start of the increase in Pb (Zillén et al., 2012) at ~8 mcd (as well as more precisely using the ^{14}C-based age model), coincides with a distinct maximum in C_{org} and maxima in Fe-sulfides, Fe_{HR}/Fe_{TOT} and $Fe_{pyrite}/Fe_{HR,}$ where the maximum in the latter might even point to some

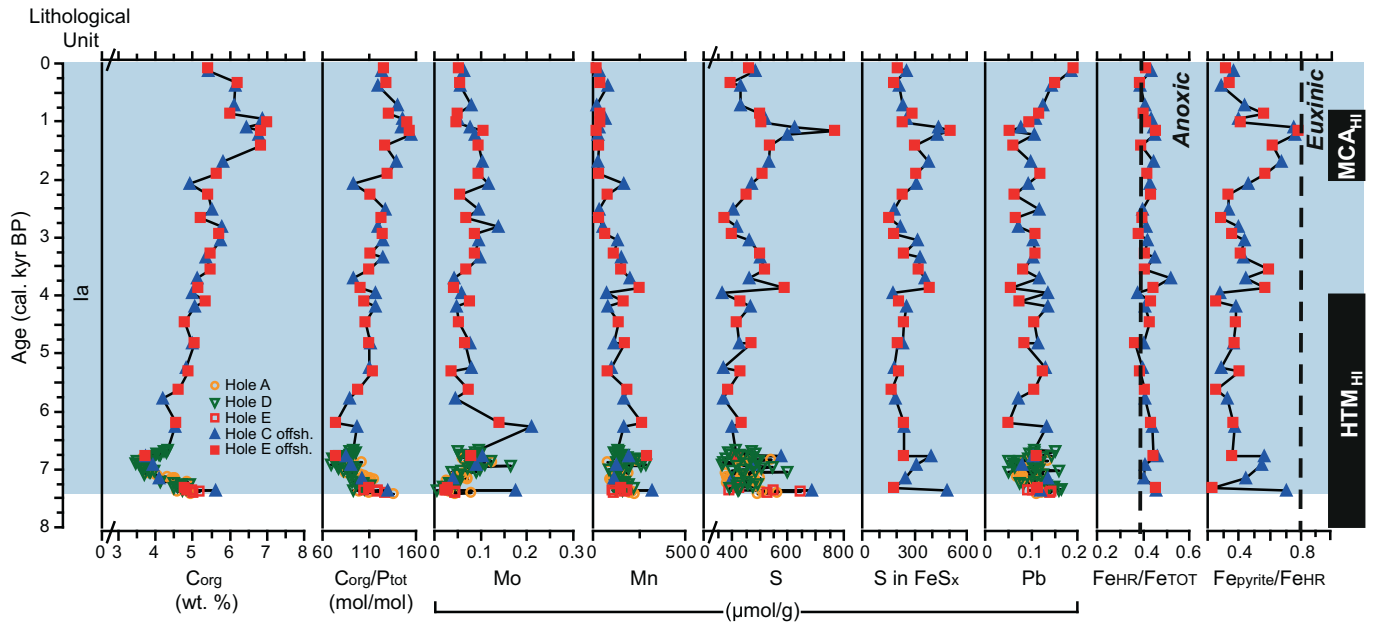

Fig. 8. Profiles of C_{org}, C_{org}/P_{tot}, Mo, Mn, S, solid phase S buried as FeSx, Pb, Fe_{HR}/Fe_{TOT} and Fe_{pyrite}/Fe_{HR} plotted against age. Lithology is shown on the left, while the timing of the previously recognized hypoxic intervals in the Baltic Sea (coinciding with the Medieval Climate Anomaly (MCA_{HI}) and Holocene Thermal Maximum (HTM_{HI}; e.g., Zillén et al., 2008)), is indicated on the right.

euxinia (März et al., 2008). This suggests that, in contrast to the coastal zone at Gåsfjärden in southeast Sweden, which was not hypoxic during the MCA period (Ning et al., 2016), at our site, the MCA was the most reducing interval of the Holocene.

In summary, the transition from freshwater lake to brackish-marine conditions did not lead to enhanced burial of C_{org} in the Little Belt. Since nutrient availability and productivity were already high before the transition to brackish-marine conditions, we infer that density stratification resulting from the inflow of denser saline waters around 8 ka was the ultimate trigger for the onset of lasting (seasonal) hypoxia in the Little Belt. Climatic warming during the HTM and MCA led to additional deoxygenation of bottom waters, resulting in the most reducing conditions. However, climatic warming seems to have played a relatively minor role in the development of hypoxia compared with the roles of high nutrient availability and density stratification.

5.5. Comparison with present-day hypoxia

Hypoxia has been steadily increasing in the coastal zone of the Baltic Sea since the 1950s (Conley et al., 2011). In the archipelagos on the Swedish east coast, hypoxia started expanding in the 1960s, and rapidly increased during the 1970–1980s (Persson and Jonsson, 2000). Recently, however, there are indications for water quality improvements and decreased hypoxia, which have been attributed to nutrient reductions (e.g., Persson and Jonsson, 2000; Karlsson et al., 2010), possibly amplified by enhanced phosphorus burial linked to the establishment of deep-burrowing macrofauna (Norkko et al., 2012). The Archipelago Sea became eutrophic in the early 1970s (Bonsdorff et al., 1997), but signs of improvement of the water quality have not been reported yet. Areas in the Danish Straits with a water depth > 17 m have been seasonally hypoxic since the 1970s (Karlson et al., 2002; Conley et al., 2007). Despite ongoing seasonal hypoxia, Andersen et al. (2015) showed a slow decline of eutrophication in the Danish Straits over the past ~15 years. Unfortunately, no surface sediments from our coring site in the Little Belt are available, preventing us from assessing the very recent history of hypoxia in the area based on sediment records. Comparison of our data with geochemical data from surface sediments from other sites in the southwestern part of the Baltic Sea and the Kattegat (Mort et al., 2010), however, shows that average sedimentary Mo concentrations for the last 8 ka in the Little Belt fall between present-day Mo concentrations for Fladen, Öresund and the Arkona Basin, which are classified as 'oxic—seasonally hypoxic', and Bornholm Basin, which is classified as 'semi-permanently hypoxic/anoxic' (Fig. 9; Mort et al., 2010). This further confirms that the Little Belt has been seasonally hypoxic ever since the transition to the brackish/marine conditions at ~8 ka BP, and suggests that it is naturally susceptible to the development of hypoxia. At present, despite the high rates of water exchange (which prevent oxygen depletion), the combination of a pycnocline at a water depth of ~15 m and a high input of nutrients and organic matter lead to oxygen depletion (Karlson et al., 2002). This demonstrates that density stratification in combination with high nutrient availability is crucial for the development of hypoxia in the Little Belt.

6. Conclusions

The Little Belt area was a well-oxygenated, oligotrophic, glacial meltwater lake prior to the Holocene. After a lowstand, possibly attributed to a sudden lowering of the water level, a short-lived phase with low oxygen conditions was followed by a freshwater lake phase. The geochemical composition of the freshwater lake sediments indicates high nutrient-availability and productivity (in contrast to the low-productivity Ancylus Lake in the central Baltic Sea), but evidence for hypoxia is absent. The transition from the freshwater lake to the brackish/marine conditions was very rapid and immediately led to (seasonally) hypoxic conditions in the Little Belt, suggesting that the density stratification associated with the salinity change was crucial for the development of hypoxia. In contrast with the deeper parts of the Baltic Sea, where hypoxia was confined to the HTM and MCA, the Little Belt remained continuously (seasonally) hypoxic after the transition from the freshwater lake to brackish/marine conditions. The most reducing conditions nevertheless correspond with the HTM and MCA.

Our results demonstrate that the response of the Little Belt to environmental perturbations during the Holocene differs from that of the deeper, offshore parts of the Baltic Sea. Climate warming only had a minor effect on the extent and degree of oxygen depletion in the Little Belt. We infer that a high natural nutrient loading (sustaining high productivity) in combination with density stratification has made the

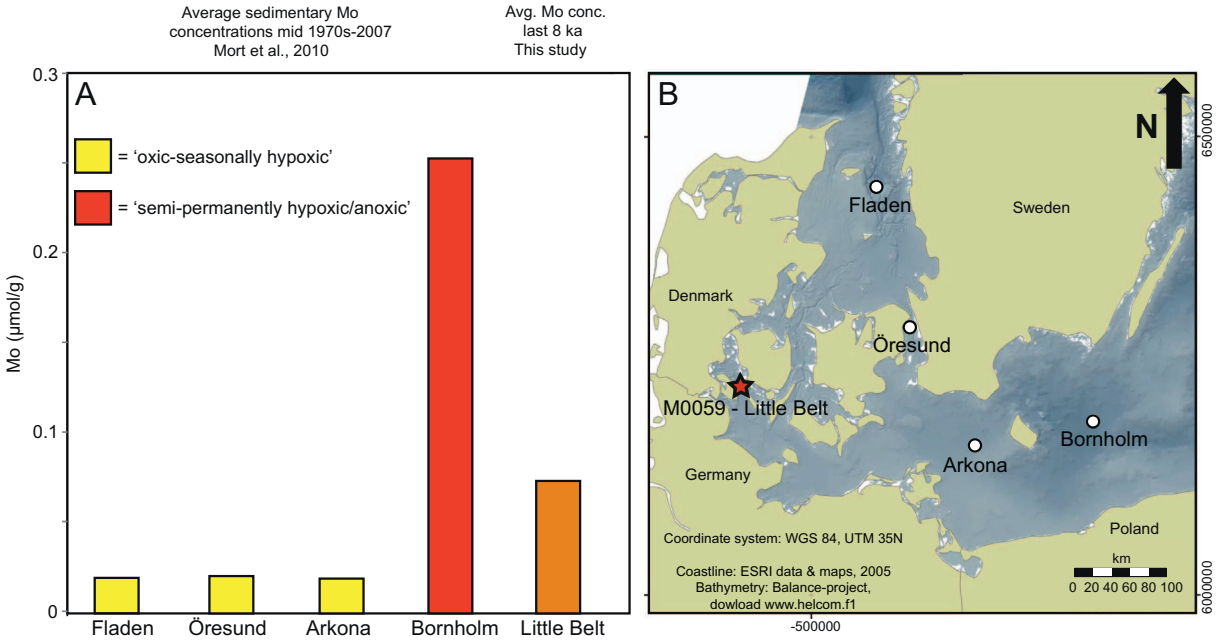

Fig. 9. Average molybdenum concentrations for the period from the mid-1970s until 2007, for the four study sites of Mort et al., 2010 that are located in the southwestern part of the Baltic Sea and the Kattegat. On the right, the average Mo concentration over the last 8 ka for the Little Belt – this study, is shown (A). Map showing the locations of the different sites (B).

Little Belt naturally susceptible to the development of (seasonal) hypoxia over the past 8 ka.

Acknowledgements

This research was funded by the European Research Council under the European Community's Seventh Framework Programme (FP7/2007–2013)/ERC Starting Grant # 278364 and the Netherlands Organisation for Scientific Research (NWO; Vici grant # 865.13.005). This work was carried out under the program of the Netherlands Earth System Science Center (NESSC), financially supported by the Ministry of Education, Culture and Science (OCW) and the BONUS COCOA project supported by BONUS (Art 185), funded jointly by the EU and FORMAS. Södertörn University provided financial support for the radiocarbon dating. B.C.L. acknowledges VR grant 637-2014-499. This research used samples provided by the Integrated Ocean Drilling Program (IODP). We thank the captain, crew and scientific participants of IODP Expedition 347. We thank Ton Zalm, Coen Mulder, Helen de Waard and Arnold van Dijk (UU) for analytical assistance and Ole Bennike (GEUS) for the identification of molluscs.

Appendix A. Supplementary data

Supplementary data to this article can be found online at http://dx.doi.org/10.1016/j.margeo.2017.03.008.

References

Algeo, T.J., Ingall, E., 2007. Sedimentary C_{org}:P ratios, paleocean ventilation, and Phanerozoic atmospheric pO_2. Palaeogeogr. Palaeoclimatol. Palaeoecol. 256, 130–155. http://dx.doi.org/10.1016/j.palaeo.2007.02.029.

Andersen, J.H., Carstensen, J., Conley, D.J., Dromph, K., Fleming, V., Gustafsson, B., Josefson, A., Norkko, A., Villnäs, A., Murray, C., 2015. Long-term temporal and spatial trends in eutrophication status of the Baltic Sea. Biol. Rev. 92, 135–149.

Anderson, T.F., Raiswell, R., 2004. Sources and mechanisms for the enrichment of highly reactive iron in euxinic Black Sea sediments. Am. J. Sci. 304 (3), 203–233.

Andrén, E., Andrén, T., Kunzendorf, H., 2000a. Holocene history of the Baltic Sea as a background for assessing records of human impact in the sediments of the Gotland Basin. The Holocene 10 (6), 687–702.

Andrén, E., Andrén, T., Sohlenius, G., 2000b. The Holocene history of the southwestern Baltic Sea as reflected in a sediment core from the Bornholm Basin. Boreas 29, 233–250.

Andrén, T., Lindeberg, G., Andrén, E., 2002. Evidence of the final drainage of the Baltic Ice Lake and the brackish phase of the Yoldia Sea in glacial varves from the Baltic Sea. Boreas 31, 226–238.

Andrén, T., Björck, S., Andrén, E., Conley, D., Lambeck, K., Zillén, L., Anjar, J., 2011. The development of the Baltic Sea basin during the last 130 ka. In: Harff, J., Björck, S., Hoth, P. (Eds.), The Baltic Sea Basin. Springer-Verlag, Berlin, pp. 75–97.

Andrén, T., Jørgensen, B.B., Cotterill, C., Expedition 347 Scientists, 2015. Integrated Ocean Drilling Program Leg 347 Initial Report. College Station, TXhttp://dx.doi.org/10.2204/iodp.proc.347.2015.

APHA, 2005. Standard Methods for the Examination of Water and Wastewater. American Public Health Association – American Water Works Association – Water Environment Federation.

Bennike, O., Jensen, J.B., 2011. Postglacial, relative shore-level changes in Lillebælt, Denmark. Geol. Surv. Denmark Greenland Bull. 23, 37–40.

Bennike, O., Jensen, J.B., 2013. A Baltic Ice Lake lowstand of latest Allerød age in the Arkona basin, southern Baltic Sea. Geol. Surv. Denmark Greenland Bull. 28, 17–20.

Berglund, B.E., 1971. Littorina transgressions in Blekinge, South Sweden a preliminary survey. GFF 93 (3), 625–652.

Berglund, B., Sandgren, P., Barnekow, L., 2005. Early Holocene history of the Baltic Sea, as reflected in coastal sediments in Blekinge, southeastern Sweden. Quat. Int. 130, 111–139.

Berner, R.A., Raiswell, R., 1983. Burial of organic carbon and pyrite sulfur in sediments over Phanerozoic time: a new theory. Geochim. Cosmochim. Acta 47 (5), 855–862. http://dx.doi.org/10.1016/0016-7037(83)90151-5.

Berner, R.A., Raiswell, R., 1984. C/S method for distinguishing freshwater from marine sedimentary rocks. Geology 12 (6), 365–368.

Björck, S., 1995. A review of the history of the Baltic Sea, 13.0–8.0 ka BP. Quat. Int. 27, 19–40.

Björck, S., Digerfeldt, G., 1989. Lake Mullsjön-a key site for understanding the final stage of the Baltic Ice Lake east of Mt. Billingen. Boreas 18 (3), 209–219.

Björck, S., Andrén, T., Jensen, J.B., 2008. An attempt to resolve the partly conflicting data and ideas on the Ancylus-Littorina transition. In: Polish Geological Institute Special Papers. 23. pp. 21–26.

Blaauw, M., 2010. Methods and code for 'classical' age-modelling of radiocarbon sequences. Quat. Geochronol. 5, 5512–5518.

Bonsdorff, E., Blomqvist, E.M., Mattila, J., Norkko, A., 1997. Coastal eutrophication: causes, consequences and perspectives in the Archipelago areas of the northern Baltic Sea. Estuar. Coast. Shelf Sci. 44 (Supplement 1), 63–72.

Böttcher, M.E., Lepland, A., 2000. Biogeochemistry of sulfur in a sediment core from the west-central Baltic Sea: evidence from stable isotopes and pyrite textures. J. Mar. Syst. 25 (3), 299–312.

Brenner, W.W., 2005. Holocene environmental history of the Gotland Basin (Baltic Sea) — a micropalaeontological model. Palaeogeogr. Palaeoclimatol. Palaeoecol. 220 (3), 227–241.

Burton, E.D., Sullivan, L.A., Bush, R.T., Johnston, S.G., Keene, A.F., 2008. A simple and inexpensive chromium-reducible sulfur method for acid-sulfate soils. Appl. Geochem. 23, 2759–2766. http://dx.doi.org/10.1016/j.apgeochem.2008.07.007.

Burton, E.D., Bush, R.T., Sullivan, L.A., Hocking, R.K., Mitchell, D.R.G., Johnston, S.G., Fitzpatrick, R.W., Raven, M., McClure, S., Jang, L.Y., 2009. Iron-monosulfide oxidation in natural sediments: resolving microbially-mediated S transformations using XANES, electron microscopy and selective extractions. Environ. Sci. Technol. 43, 3128–3134.

Carstensen, J., Andersen, J.H., Gustafsson, B.G., Conley, D.J., 2014a. Deoxygenation of

the Baltic Sea during the last century. Proc. Natl. Acad. Sci. U. S. A. 111, 5628–5633. http://dx.doi.org/10.1073/pnas.1323156111.
Carstensen, J., Conley, D.J., Bonsdorff, E., Gustafsson, B.G., Hietanen, S., Janas, U., Jilbert, T., Maximov, A., Norkko, A., Norkko, J., Reed, D.C., Slomp, C.P., Timmermann, K., Voss, M., 2014b. Hypoxia in the Baltic Sea: biogeochemical cycles, benthic fauna, and management. Ambio 43, 26–36.
Chappaz, A., Gobeil, C., Tessier, A., 2008. Geochemical and anthropogenic enrichments of Mo in sediments from perennially oxic and seasonally anoxic lakes in Eastern Canada. Geochim. Cosmochim. Acta 72 (1), 170–184.
Conley, D.J., Carstensen, J., Ærtebjerg, G., Christensen, P.B., Dalsgaard, T., Hansen, J.L.S., Josefson, A.B., 2007. Long-term changes and impacts of hypoxia in Danish coastal waters. Ecol. Appl. 17, S165–S184.
Conley, D.J., Björck, S., Bonsdorff, E., Carstensen, J., Destouni, G., Gustafsson, B.G., Hietanen, S., Kortekaas, M., Kuosa, H., Markus Meier, H.E., Müller-Karulis, B., Nordberg, K., Norkko, A., Nürnberg, G., Pitkänen, H., Rabalais, N.N., Rosenberg, R., Savchuk, O.P., Slomp, C.P., Voss, M., Wulff, F., Zillén, L., 2009. Hypoxia-related processes in the Baltic Sea. Environ. Sci. Technol. 43, 3412–3420. http://dx.doi.org/10.1021/es802762a.
Conley, D.J., Carstensen, J., Aigars, J., Axe, P., Bonsdorff, E., Eremina, T., Haahti, B.M., Humborg, C., et al., 2011. Hypoxia is increasing in the coastal zone of the Baltic Sea. Environ. Sci. Technol. 45, 6777–6783.
Diaz, R.J., Rosenberg, R., 2008. Spreading dead zones and consequences for marine ecosystems. Science 321, 926–929. http://dx.doi.org/10.1126/science.1156401.
Dijkstra, N., Slomp, C.P., Behrends, T., 2016. Vivianite is a key sink for phosphorus in sediments of the Landsort Deep, an intermittently anoxic deep basin in the Baltic Sea. Chem. Geol. 438, 58–72.
Egger, M., Rasigraf, O., Sapart, C.J., Jilbert, T., Jetten, M.S.M., Röckmann, T., van der Veen, C., Bånda, N., Kartal, B., Ettwig, K.F., Slomp, C.P., 2015. Iron-mediated anaerobic oxidation of methane in brackish coastal sediments. Environ. Sci. Technol. 49, 277–283.
Ekdale, A.A., Mason, T.R., 1988. Characteristic trace-fossil associations in oxygen-poor sedimentary environments. Geology 16 (8), 720–723.
Emerson, S.R., Huested, S.S., 1991. Ocean anoxia and the concentrations of molybdenum and vanadium in seawater. Mar. Chem. 34 (3), 177–196. http://dx.doi.org/10.1016/0304-4203(91)90002.
Esper, J., Cook, E.R., Schweingruber, F.H., 2002. Low-frequency signals in long tree-ring chronologies for reconstructing past temperature variability. Science 295, 2250–2253.
Frietsch, R., Papunen, H., Vokes, F.M., 1979. The ore deposits in Finland, Norway, and Sweden; a review. Econ. Geol. 74 (5), 975–1001.
Gustafsson, B.G., Westman, P., 2002. On the causes for salinity variations in the Baltic Sea during the last 8500 years. Paleoceanography 17 (3).
Gustafsson, B.G., Schenk, F., Blenckner, T., Eilola, K., Meier, H.E.M., Müller-Karulis, B., Neumann, T., Ruoho-Airola, T., Savchuk, O.P., Zorita, E., 2012. Reconstructing the development of Baltic Sea eutrophication 1850–2006. Ambio 41 (6), 534–548. http://dx.doi.org/10.1007/s13280-012-0318-x.
Hallegraeff, G.M., 2010. Ocean climate change, phytoplankton community responses, and harmful algal blooms: a formidable predictive challenge1. J. Phycol. 46 (2), 220–235.
Heier-Nielsen, S., Heinemeir, J., Nielsen, H.L., Rud, N., 1995. Recent reservoir ages for Danish fjords and marine waters. Radiocarbon 37, 875–882.
Helz, G.R., Miller, C.V., Charnock, J.M., Mosselmans, J.F.W., Pattrick, R.A.D., Garner, C.D., Vaughan, D.J., 1996. Mechanism of molybdenum removal from the sea and its concentration in black shales: EXAFS evidence. Geochim. Cosmochim. Acta 60, 3631–3642. http://dx.doi.org/10.1016/0016-7037(96)00195-0.
Houmark-Nielsen, M., Kjaer, K.H., 2003. Southwest Scandinavia, 40–15 kyr BP: palaeogeography and environmental change. J. Quat. Sci. 18 (8), 769–786.
Huckriede, H., Meischner, D., 1996. Origin and environment of manganese-rich sediments within black-shale basins. Geochim. Cosmochim. Acta 60 (8), 1399–1413. http://dx.doi.org/10.1016/0016-7037(96)00008-7.
Jakobsson, M., Björck, S., Alm, G., Andrén, T., Lindeberg, G., Svensson, N.O., 2007. Reconstructing the Younger Dryas ice dammed lake in the Baltic Basin: bathymetry, area and volume. Glob. Planet. Chang. 57, 355–370.
Hutchinson, G.E., 1973. Marginalia: eutrophication: the scientific background of a contemporary practical problem. Am. Sci. 61.3, 269–279.
Jensen, J.B., Bennike, O., Witkowski, A., Lemke, W., Kuijpers, A., 1999. Early Holocene history of the southwestern Baltic Sea: the Ancylus Lake stage. Boreas 28, 437–453.
Jilbert, T., Slomp, C.P., 2013. Rapid high-amplitude variability in Baltic Sea hypoxia during the Holocene. Geology 41, 1183–1186. http://dx.doi.org/10.1130/G34804.1.
Jilbert, T., Conley, D.J., Gustafsson, B.G., Funkey, C.P., Slomp, C.P., 2015. Glacio-isostatic control on hypoxia in a high-latitude shelf basin. Geology 43 (5), 427–430.
Jørgensen, B.B., Böttcher, M.E., Lüschen, H., Neretin, L.N., Volkov, I.I., 2004. Anaerobic methane oxidation and a deep H_2S sink generate isotopically heavy sulfides in Black Sea sediments. Geochim. Cosmochim. Acta 68 (9), 2095–2118.
Kabel, K., Moros, M., Porsche, C., Neumann, T., Adolphi, F., Andersen, T.J., Siegel, H., Gerth, M., Leipe, T., Jansen, E., Sinninghe Damsté, J.S., 2012. Impact of climate change on the Baltic Sea ecosystem over the past 1,000 years. Nat. Clim. Chang. 2, 871–874. http://dx.doi.org/10.1038/nclimate1595.
Karlson, K., Rosenberg, R., Bonsdorff, E., 2002. Temporal and spatial large-scale effects of eutrophication and oxygen deficiency on benthic fauna in Scandinavian and Baltic waters: a review. Oceanogr. Mar. Biol. 40, 427–489.
Karlsson, O.M., Jonsson, P., Lindgren, D., Malmaeus, J.M., Stehn, A., 2010. Indications of recovery of hypoxia in the Inner Stockholm Archipelago. Ambio 39, 486–495.
Karstensen, J., Fiedler, B., Schütte, F., Brandt, P., Körtzinger, A., Fischer, G., Zantopp, R., Hahn, J., Visbeck, M., Wallace, D., 2015. Open ocean dead zones in the tropical North Atlantic Ocean. Biogeosciences 12, 2597–2605. http://dx.doi.org/10.5194/bg-12-2597-2015.
Keeling, R.F., Körtzinger, A., Gruber, N., 2010. Ocean deoxygenation in a warming world. Annu. Rev. Mar. Sci. 2, 199–229.
Kraal, P., Slomp, C.P., Forster, A., Kuypers, M.M., Sluijs, A., 2009. Pyrite oxidation during sample storage determines phosphorus fractionation in carbonate-poor anoxic sediments. Geochim. Cosmochim. Acta 73 (11), 3277–3290.
Lenz, C., Jilbert, T., Conley, D.J., Slomp, C.P., 2015. Hypoxia-driven variations in iron and manganese shuttling in the Baltic Sea over the past 8 kyr. Geochem. Geophys. Geosyst. 16 (10), 3754–3766.
Lougheed, B.C., Snowball, I., Moros, M., Kabel, K., Muscheler, R., Virtasalo, J.J., Wacker, L., 2012. Using an independent geochronology based on palaeomagnetic secular variation (PSV) and atmospheric Pb deposition to date Baltic Sea sediments and infer ^{14}C reservoir age. Quat. Sci. Rev. 42, 43–58.
Lougheed, B.C., Filipsson, H.L., Snowball, I., 2013. Large spatial variations in coastal ^{14}C reservoir age - a case study from the Baltic Sea. Clim. Past 9, 1015–1028.
März, C., Poulton, S.W., Beckmann, B., Küster, K., Wagner, T., Kasten, S., 2008. Redox sensitivity of P cycling during marine black shale formation: dynamics of sulfidic and anoxic, non-sulfidic bottom waters. Geochim. Cosmochim. Acta 72, 3703–3717.
Melkerud, P.A., Bain, D.C., Jongmans, A.G., Tarvainen, T., 2000. Chemical, mineralogical and morphological characterization of three podzols developed on glacial deposits in Northern Europe. Geoderma 94 (2), 125–148.
Meyer, M., Harff, J., 2005. Modelling palaeo coastline changes of the Baltic Sea. J. Coast. Res. 598–609.
Mort, H.P., Slomp, C.P., Gustafsson, B.G., Andersen, T.J., 2010. Phosphorus recycling and burial in Baltic Sea sediments with contrasting redox conditions. Geochim. Cosmochim. Acta 74, 1350–1362.
Neumann, T., Christiansen, C., Clasen, S., Emeis, K.C., Kunzendorf, H., 1997. Geochemical records of salt-water inflow into the deep basins of the Baltic Sea. Cont. Shelf Res. 17, 95–115.
Ning, W., Ghosh, A., Jilbert, T., Slomp, C.P., Khan, M., Nyberg, J., Conley, D.J., Filipsson, H.L., 2016. Evolving coastal character of a Baltic Sea inlet during the Holocene shoreline regression: impact on coastal zone hypoxia. J. Paleolimnol. 55 (4), 319–338.
Norkko, J., Reed, D.C., Timmermann, K., Norkko, A., Gustafsson, B.G., Bonsdorff, E., Slomp, C.P., Carstensen, J., Conley, D.J., 2012. A welcome can of worms? Hypoxia mitigation by an invasive species. Glob. Chang. Biol. 18, 422–434.
Obrochta, S.P., Crowley, T.J., Channell, J.E.T., Hodell, D.A., Baker, P.A., Seki, A., Yokoyama, Y., 2014. Climate variability and ice-sheet dynamics during the last three glaciations. Earth Planet. Sci. Lett. 406 (0), 198–212.
Persson, J., Jonsson, P., 2000. Historical development of laminated sediments—an approach to detect soft sediment ecosystem changes in the Baltic Sea. Mar. Pollut. Bull. 40, 122–134.
Poulton, S.W., Canfield, D.E., 2005. Development of a sequential extraction procedure for iron: implications for iron partitioning in continentally derived particulates. Chem. Geol. 214, 209–221. http://dx.doi.org/10.1016/j.chemgeo.2004.09.003.
Poulton, S.W., Canfield, D.E., 2011. Ferruginous conditions: a dominant feature of the ocean through Earth's history. Elements 7 (2), 107–112.
Poulton, S.W., Raiswell, R., 2002. The low temperature geochemical cycle of iron: from continental fluxes to marine sediment deposition. Am. J. Sci. 302, 774–805.
Rabalais, N.N., Turner, R.E., Wiseman Jr., W.J., 2002. Gulf of Mexico hypoxia, aka "The dead zone". Annu. Rev. Ecol. Syst. 235–263.
Raiswell, R., Canfield, D.E., 1998. Sources of iron for pyrite formation in marine sediments. Am. J. Sci. 298, 219–245.
Reed, D.C., Slomp, C.P., de Lange, G.J., 2011. A quantitative reconstruction of organic matter and nutrient diagenesis in Mediterranean Sea sediments over the Holocene. Geochim. Cosmochim. Acta 75, 5540–5558. http://dx.doi.org/10.1016/j.gca.2011.07.002.
Reimer, P.J., Bard, E., Bayliss, A., Beck, J.W., Blackwell, P.G., Bronk Ramsey, C., Buck, C.E., Cheng, H., Edwards, R.L., Friedrich, M., Grootes, P.M., Guilderson, T.P., Haflidason, H., Hajdas, I., Hatté, C., Heaton, T.J., Hoffmann, D.L., Hogg, A.G., Hughen, K.A., Kaiser, K.F., Kromer, B., Manning, S.W., Niu, M., Reimer, R.W., Richards, D.A., Scott, E.M., Southon, J.R., Staff, R.A., Turney, C.S.M., van der Plicht, J., 2013. IntCal13 and Marine13 radiocarbon age calibration curves 0–50,000 years cal BP. Radiocarbon 55, 1869–1887.
Reinholdsson, M., Snowball, I., Zillén, L., Lenz, C., Conley, D.J., 2013. Magnetic enhancement of Baltic Sea sapropels by greigite magnetofossils. Earth Planet. Sci. Lett. 366, 137–150.
Renssen, H., Seppä, H., Crosta, X., Goosse, H., Roche, D.M., 2012. Global characterization of the Holocene thermal maximum. Quat. Sci. Rev. 48, 7–19.
Rickard, D.T., 1979. Scandinavian metallogenesis. GeoJournal 3 (3), 235–252.
Schaller, T., Moor, H.C., Wehrli, B., 1997. Sedimentary profiles of Fe, Mn, V, Cr, As and Mo as indicators of benthic redox conditions in Baldeggersee. Aquat. Sci. 59 (4), 345–361.
Scott, C., Lyons, T.W., 2012. Contrasting molybdenum cycling and isotopic properties in euxinic versus non-euxinic sediments and sedimentary rocks: refining the paleoproxies. Chem. Geol. 324-325, 19–27.
Snowball, I.F., Korhola, A., Briffa, K.R., Koç, N., 2004. Holocene climate dynamics in Fennoscandia and the North Atlantic. In: Battarbee, R.W., Gasse, F., Stickley, C.E. (Eds.), Past Climate Variability Through Europe and Africa. Springer, Dordrecht, the Netherlands, pp. 465–494.
Sohlenius, G., Sternbeck, J., Andrén, E., Westman, P., 1996. Holocene history of the Baltic Sea as recorded in a sediment core from the Gotland Deep. Mar. Geol. 134, 183–201.
Sohlenius, G., Emeis, K.C., Andrén, E., Andrén, T., Kohly, A., 2001. Development of anoxia during the fresh–brackish water transition in the Baltic Sea. Mar. Geol. 177, 221–242.
Stigebrandt, A., Gustafsson, B.G., 2003. Response of the Baltic Sea to climate change-theory and observations. J. Sea Res. 49 (4), 243–256.

Stramma, L., Johnson, G.C., Sprintall, J., Mohrholz, V., 2008. Expanding oxygen-minimum zones in the tropical oceans. Science 320, 655–658.
Vaquer-Sunyer, R., Duarte, C.M., 2008. Thresholds of hypoxia for marine biodiversity. Proc. Natl. Acad. Sci. U. S. A. 105, 15452–15457.
Walker, M., Johnsen, S., Rasmussen, S., Popp, T., Steffensen, J.P., Gibbard, P., Hoek, W., Lowe, J., Andrews, J., Björck, S., Cwynar, L., Hughen, K., Kershaw, P., Kromer, B., Litt, T., Lowe, D., Nakagawa, T., Newnham, R., Schwander, J., 2009. Formal definition and dating of the GSSP (Global Stratotype Section and Point) for the base of the Holocene using the Greenland NGRIP ice core, and selected auxiliary records. J. Quat. Sci. 24, 3–17.
Whitney, F.A., Freeland, H.J., Robert, M., 2007. Persistently declining oxygen levels in the interior waters of the eastern subarctic Pacific. Prog. Oceanogr. 75 (2), 179–199.
Widerlund, A., Andersson, P.S., 2011. Late Holocene freshening of the Baltic Sea derived from high-resolution strontium isotope analyses of mollusk shells. Geology 39 (2), 187–190.
Wulff, F., Stigebrandt, A., Rahm, L., 1990. Nutrient dynamics of the Baltic Sea. Ambio 19, 126–133.
Zillén, L., Conley, D.J., 2010. Hypoxia and cyanobacteria blooms—are they really natural features of the late Holocene history of the Baltic Sea? Biogeosciences 7, 2567–2580. http://dx.doi.org/10.5194/bg-7-2567-2010.
Zillén, L., Conley, D.J., Andrén, T., Andrén, E., Björck, S., 2008. Past occurrences of hypoxia in the Baltic Sea and the role of climate variability, environmental change and human impact. Earth Sci. Rev. 91, 77–92. http://dx.doi.org/10.1016/j.earscirev.2008.10.001.
Zillén, L., Lenz, C., Jilbert, T., 2012. Stable lead (Pb) isotopes and concentrations – A useful independent dating tool for Baltic Sea sediments. Quat. Geochronol. 8, 41–45.